Quantum algorithm for evaluating operator size with Bell measurements

Xi-Dan Hu [1], Tong Luo [1], and Dan-Bo Zhang [2,1,*]

[1]*Guangdong Provincial Key Laboratory of Quantum Engineering and Quantum Materials,*
School of Physics and Telecommunication Engineering, South China Normal University, Guangzhou 510006, China
[2]*Guangdong-Hong Kong Joint Laboratory of Quantum Matter, Frontier Research Institute for Physics,*
South China Normal University, Guangzhou 510006, China

Operator size growth describes the scrambling of operators in quantum dynamics and stands out as an essential physical concept for characterizing quantum chaos. Important as it is, a scheme for the direct measuring of operator size on a quantum computer is still absent. Here, we propose a quantum algorithm for the direct measuring of the operator size and its distribution based on Bell measurement. The algorithm is verified with spin chains and, meanwhile, the effects of Trotterization error and quantum noise are analyzed. It is revealed that saturation of operator size growth can be due to quantum chaos itself or be a consequence of quantum noise. Nevertheless, it is found that the error mitigation will effectively reduce the influence of noise, so as to restore the distinguishability of oscillation and saturation behaviors of operator scrambling. Our work provides a feasible protocol for investigating quantum chaos on noisy quantum computers by measuring operator size growth.

I. INTRODUCTION

Characterizing quantum chaos has drawn intensive interest in recent years due to its fundamental role in understanding quantum statistical mechanics [1–3]. One important perspective to study quantum chaos is to investigate the quantum information scrambling [4–10], a concept to describe how local information can be scrambled into the whole system and become nonlocal. The information scrambling can be quantified by the out-of-time-ordered correlations (OTOCs) [11–18]. Remarkably, recent rapid advances in quantum processors enable us to observe information scrambling by measuring OTOCs [9,13,19,20], which is unusual as typical correlation functions are time ordered.

An alternative approach to understand information scrambling is to directly investigate the operator spreading [21–32]. In this picture, a local operator after evolution can spread into a linear combination of highly nonlocal operators, and the number of nonlocal operators can be exponentially enlarged, making extraction of information encoded in the initial local operator impractical. In other words, the operator size can grow with time until reaching the system size. The operator size growth can be intuitive for characterizing and understanding quantum chaotic systems. Remarkably, for open-system dynamics where OTOCs can have difficulty telling information scrambling of the evolution of the system itself apart from noises of the environment, the operator size distribution can still give a faithful characterization. In this regard, operator size growth provides a promising avenue to study information scrambling other than OTOCs. However, there is still a lack of feasible schemes to directly measure the operator size

on quantum processors, except for indirect measurement by inferring from data obtained by quantum quenches from an ensemble of random initial states [9,27].

In this paper, we propose a quantum algorithm that can directly measure the operator size and its distribution, which is feasible on near-term quantum computers. The scheme is based on a mapping between Pauli operators and Bell states. By preparing a product of Bell states, the operator of Heisenberg evolution will imprint the information of the product of Pauli operators into Bell states, and by Bell measurements, the operator size and its distribution can be extracted. In the numerical simulation, we consider both Trotterization error and quantum noises that are related to implementation. For spin chains, it is found that quantum noises may make the different behaviors between integrable chain and quantum chaotic chain [27] tend to disappear, as for both the operator sizes grow to saturation. Nevertheless, we show that the feature of operator size oscillation can be restored for the integrable system by error mitigation [33–38]. Our work points out that the operator scrambling by measuring the operator size can be feasible on near-term quantum devices with error mitigation.

The paper is organized as follows. In Sec. II, we introduce the definition of operator size and propose a quantum algorithm based on Bell measurements to evaluate the operator size. Then, in Sec. III, we present numerical simulation results for spin chains and analyze the effects of Trotterization, quantum noise, and error mitigation. Finally, we make conclusions in Sec. IV.

II. EVALUATING OPERATOR SIZE BY BELL MEASUREMENTS

In this section, we first give a definition of operator size for quantum systems. Then, we illustrate how Bell measurements

---

*dbzhang@m.scnu.edu.cn

can be exploited to measure the operator size. We mention that recently Bell measurement has had broad applications in quantum information science, such as for estimating Pauli channels [39], learning quantum experiments [40], and measuring the degree of magic of nonstabilizer states [41].

A. Operator size

To be concrete without loss of generality, we consider a lattice model where each site is a qubit (spin half). The Hamiltonian can be written as a summation of local terms, $H = \sum_i \lambda_i H_i$, with each local term H_i a product of Pauli operators. In the Heisenberg picture, the time evolution of a quantum system can be encapsulated into the time-dependent operator $\hat{O}(t)$, which satisfies the equation of motion,

$$\frac{\partial \hat{O}(t)}{\partial t} = i[\hat{H}, \hat{O}(t)]. \tag{1}$$

The solution is $\hat{O}(t) = e^{i\hat{H}t}\hat{O}(0)e^{-i\hat{H}t}$.

The time evolution of quantum systems can be very complicated, even if the Hamiltonian itself is simple and the initial operator $\hat{O}(0)$ is a single Pauli operator. To see this, the operator $\hat{O}(t)$ can be written as

$$\hat{O}(t) = \left[\sum_{n=0}^{\infty} \frac{(i\hat{H}t)^n}{n!}\right] \hat{O}(0) \left[\sum_{n=0}^{\infty} \frac{(-i\hat{H}t)^n}{n!}\right]. \tag{2}$$

For a generic quantum many-body system, a single Pauli operator can evolve into a linear combination of products of Pauli operators, which may involve many operators by expanding H^n in Eq. (2).

For a generic N-qubit lattice system, the operator $\hat{O}(t)$ can be written under the Pauli basis (product of Pauli operators),

$$\hat{O}(t) = \sum_{\mathbf{k}=0}^{4^N-1} C_{\mathbf{k}}(t)\hat{P}_{\mathbf{k}}, \quad \hat{P}_{\mathbf{k}} = \bigotimes_{n=1}^{N} \sigma_n^{k_n}. \tag{3}$$

Here we have used a quaternary number $\mathbf{k} = k_1 k_2, \ldots, k_N$ ($k_n = 0, 1, 2, 3$) to label all Pauli bases in order and Pauli matrices are $\sigma^0 = I$, $\sigma^1 = X$, $\sigma^2 = Y$, $\sigma^3 = Z$. The coefficient can be evaluated as

$$C_{\mathbf{k}}(t) = 2^{-N}\text{tr}[\hat{O}(t)\hat{P}_{\mathbf{k}}]. \tag{4}$$

Once the initial operator $\hat{O}(0)$ is Hermitian, it can be seen that $\hat{O}(t)$ is Hermitian and all coefficients $C_{\mathbf{k}}(t)$ are real numbers. Thus, it requires 4^N real numbers to fully characterize the operator $\hat{O}(t)$, which becomes inaccessible for a generic quantum many-body system due to the exponential growth. Nevertheless, one may study some properties of $\hat{O}(t)$ that are of physical interest.

From the aspect of quantum information scrambling, one remarkable feature of $\hat{O}(t)$ is to investigate how the operator size is growing with time evolution. For quantum chaos, the initial local information can be scrambled into the whole system. The information is distributed extensively in the system and thus becomes nonlocal. The Pauli basis is suitable to study the degree of extensiveness by defining its operator size, which counts how many non-I operators are in $\hat{P}_{\mathbf{k}}$. Initially, the operator size $\hat{O}(0)$ as a Pauli operator on a site is one. With the time evolution, the operator $\hat{O}(t)$ is a superposition of the

Pauli basis with different operator sizes, and it is necessary to use an averaged operator size. For quantum chaos, the averaged operator size grows with time until saturation, which is $O(L)$.

Let us explicitly write the averaged operator size, which is

$$L[\hat{O}(t)] \equiv \sum_{\mathbf{k}=0}^{4^N-1} |C_{\mathbf{k}}(t)|^2 \times l_{\hat{P}_{\mathbf{k}}}. \tag{5}$$

Here, $l_{\hat{P}_{\mathbf{k}}}$ is the operator size of Pauli basis $\hat{P}_{\mathbf{k}}$ defined as

$$l_{\hat{P}_{\mathbf{k}}} = \sum_{n=1}^{N} S(\sigma_n^{k_n}), \tag{6}$$

where $S(I) = 0$, $S(X) = S(Y) = S(Z) = 1$. Equivalently, $l_{\hat{P}_{\mathbf{k}}}$ can be obtained by counting the number of nonzeros in the quaternary number $\mathbf{k} = k_1 k_2 \ldots k_N$ [27]. It is noted that the operator size expressed in Eq. (5) is a measure of the operator itself and is state independent. Another definition of operator size, which is state dependent, can be found in Refs. [23,24].

B. Bell measurements

We first introduce some interesting properties of Bell states related to Pauli operators. Then, a scheme for measuring the operator size is given.

The Bell states are two-qubit maximally entangled states. There are four Bell states (Bell basis), which are given as follows:

$$\begin{aligned}
\left|B_n^0\right\rangle &= \frac{1}{\sqrt{2}}(|0_n 0_{n'}\rangle + |1_n 1_{n'}\rangle), \\
\left|B_n^x\right\rangle &= X_n\left|B_n^0\right\rangle = \frac{1}{\sqrt{2}}(|1_n 0_{n'}\rangle + |0_n 1_{n'}\rangle), \\
\left|B_n^y\right\rangle &= Y_n\left|B_n^0\right\rangle = \frac{i}{\sqrt{2}}(|1_n 0_{n'}\rangle - |0_n 1_{n'}\rangle), \\
\left|B_n^z\right\rangle &= Z_n\left|B_n^0\right\rangle = \frac{1}{\sqrt{2}}(|0_n 0_{n'}\rangle - |1_n 1_{n'}\rangle),
\end{aligned} \tag{7}$$

where X_n, Y_n, Z_n is the corresponding quantum gate on the qubit n and n' represents the ancillary qubit. The four Bell bases are orthogonal to each other. Thus, a mapping can be established between four Pauli operators $\{I, X, Y, Z\}$ and four Bell states $\{|B^0\rangle, |B^x\rangle, |B^z\rangle, |B^z\rangle\}$, respectively. For convenience, we interchangeably use the notions $|B_n^x\rangle = |B_n^1\rangle$, $|B_n^y\rangle = |B_n^2\rangle$, $|B_n^z\rangle = |B_n^3\rangle$.

The imprinting of information of Pauli operators into Bell states can be generalized into a Pauli basis. For instance, considering a two-qubit system and an operator

$$\hat{O}_f = C_0 I_1 I_2 + C_1 X_1 I_2 + C_4 I_1 X_2 + C_7 Z_1 X_2, \tag{8}$$

one can perform $\hat{O}_f$ on an initial $|B_1^0 B_2^0\rangle$, which leads to

$$|\psi_f\rangle = C_0|B_1^0 B_2^0\rangle + C_1|B_1^1 B_2^0\rangle + C_4|B_1^0 B_2^1\rangle + C_7|B_1^3 B_2^1\rangle. \tag{9}$$

Now, each Pauli basis is mapped into a product of a Bell basis (General Bell basis). The operator size can be obtained by counting the number of Bell basis that is not $|B^0\rangle$ in the general Bell basis, which can be implemented with projective
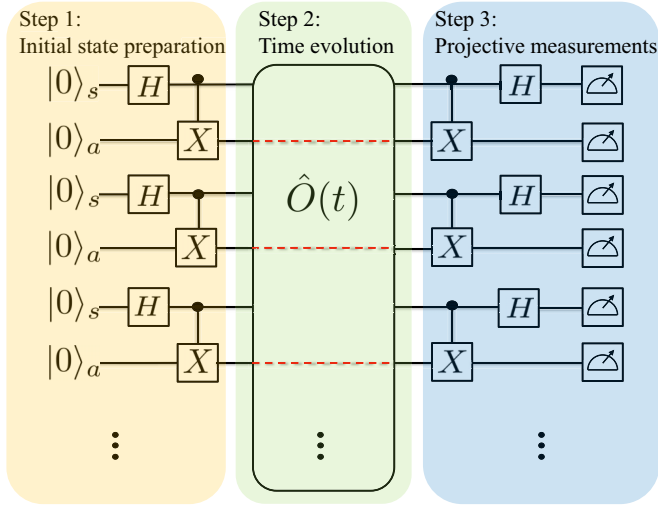
FIG. 1. The schematic diagram for the quantum circuit to calculate the operator size of operator $\hat{O}(t)$. Here, $|0\rangle_s$ and $|0\rangle_a$ represent the system qubit and the auxiliary qubit, respectively. The $\hat{O}(t)$ operator implements only on the system qubits.

measurements. One can evaluate the average operator size as

$$L[\hat{O}_f] = |C_0|^2 \times 0 + (|C_1|^2 + |C_4|^2) \times 1 + |C_7|^2 \times 2. \quad (10)$$

A generalization to an N-qubit system can be straightforward.

Now we present a procedure to evaluate the operator size with Bell measurements, which consists of three main steps (also illustrated in Fig. 1).

Step 1: Initial state preparation. Prepare the initial state as a product of N Bell states,

$$|\psi_0\rangle = \bigotimes_{n=1}^{N} |B_n^0\rangle. \quad (11)$$

For an N-qubit quantum system, a total $2N$ qubits is required.

Step 2: Time evolution. Perform the unitary operator $\hat{O}(t) = e^{i\hat{H}t}\hat{O}(0)e^{-i\hat{H}t}$ on the initial state $|\psi_0\rangle$, and one gets

$$|\psi(t)\rangle = \hat{O}(t)|\psi_0\rangle$$

$$= \sum_{\mathbf{k}=0}^{4^N-1} C_{\mathbf{k}}(t)\hat{P}_{\mathbf{k}}|\psi_0\rangle$$

$$= \sum_{\mathbf{k}=0}^{4^N-1} C_{\mathbf{k}}(t)\bigotimes_{n=1}^{N} |B_n^{k_n}\rangle$$

$$= \sum_{\mathbf{k}=0}^{4^N-1} C_{\mathbf{k}}(t)|\mathbf{k}\rangle, \quad (12)$$

where we have denoted $|\mathbf{k}\rangle \equiv \bigotimes_{n=1}^{N} |B_n^{k_n}\rangle$.

Step 3: Projective measurements. Perform the projective measurement,

$$\hat{M} = \sum_{n=1}^{N} \hat{M}_n, \quad \hat{M}_n = 1 - |B_n^0\rangle\langle B_n^0|. \quad (13)$$

The expectation value of $\hat{M}$ is equal to the averaged operator size $L[\hat{O}(t)]$, which is derived from the following:

$$\langle\psi(t)|\hat{M}|\psi(t)\rangle = \sum_{\mathbf{k}=0}^{4^N-1} |C_{\mathbf{k}}(t)|^2 \langle\mathbf{k}|\hat{M}|\mathbf{k}\rangle$$

$$= \sum_{\mathbf{k}=0}^{4^N-1} |C_{\mathbf{k}}(t)|^2 \sum_{n=1}^{N} S(k_n)$$

$$= \sum_{\mathbf{k}=0}^{4^N-1} |C_{\mathbf{k}}(t)|^2 l_{\hat{P}_{\mathbf{k}}} = L[\hat{O}(t)]. \quad (14)$$

Here, $S(k_n) = \langle\mathbf{k}|\hat{M}_n|\mathbf{k}\rangle$ with $S(0) = 0, S(1) = S(2) = S(3) = 1$. As $S(k_n) = S(\sigma_n^{k_n})$, we have $\sum_{n=1}^{N} S(k_n) = \sum_{n=1}^{N} S(\sigma_n^{k_n}) = l_{\hat{P}_{\mathbf{k}}}$.

The procedure of initial state preparation, time evolution, and projective measurement should be repeated to evaluate $L[\hat{O}(t)]$ with an acceptable statistical error. Some remarks are in order. First, the Hamiltonian evolution $e^{-i\hat{H}t}$ for the Hamiltonian H and its reversion $e^{i\hat{H}t}$ may be implemented directly on an analog quantum simulator by engineering the Hamiltonian H and $-H$, respectively. For a digital quantum computer, the evolution should be decomposed into sequences of quantum gates by Trotterization. Here we focus on the digital quantum simulation. Second, by performing measurement $\hat{M}$, one can also access the distribution of operator size, which takes integer values $M = 0, 1, 2, \ldots, N$. Third, the projective measurement can be decomposed as

$$\sum_{n=1}^{N} \langle\psi(t)|\hat{M}_n|\psi(t)\rangle = \sum_{n=1}^{N} L_n[\hat{O}(t)], \quad (15)$$

where $L_n[\hat{O}(t)]$ can be taken as the operator density at site n for the operator $\hat{O}(t)$. Thus, the averaged operator size is a summation of local operator densities.

III. SIMULATION RESULTS

In this section, we demonstrate the quantum algorithm using a model Hamiltonian with numerical simulations. We consider both the Trotterization error and quantum noise, which are two necessary ingredients when implementing the quantum algorithm. The numerical simulation is conducted using the open-source package QIBO.

As an example, we consider the mixed-field Ising model (MFIM), which is a typical quantum chaotic system. The Hamiltonian of the MFIM reads

$$\hat{H}_I = \sum_{n=1}^{N-1} J Z_n Z_{n+1} + h_x \sum_{n=1}^{N} X_n + h_z \sum_{n=1}^{N} Z_n. \quad (16)$$

The MFIM reduces to the transverse-field Ising model (TFIM) at $h_z = 0$, which is an integrable system. In the demonstration, the system size is taken as $N = 5$ and the operator that is investigated is $X_3(t)$. This takes 10 qubits in the quantum computation as one Bell state needs two qubits.

In the ideal situation where both Trotter error and quantum noise are ignored, the results of operator size growth for both the MFIM ($h_z \neq 0$) and TFIM ($h_z = 0$) are shown
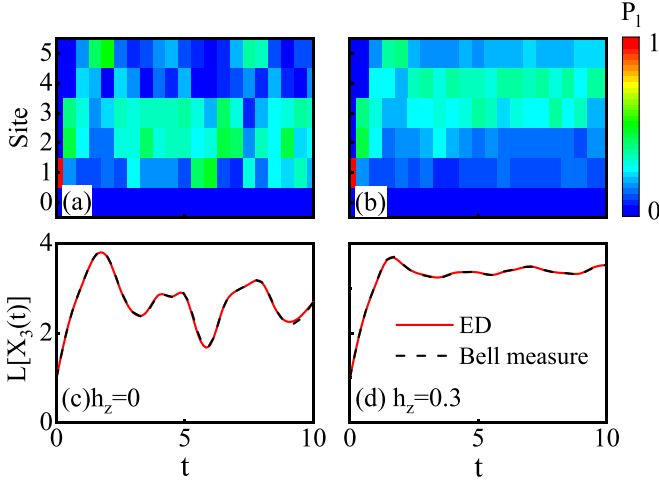
FIG. 2. The operator size of $X_3(t)$ for the quantum Ising model with system site $N = 5$. (a) The operator size distribution of the integrable system ($h_z = 0$) with different time t. (b) The quantum chaotic one ($h_z = 0.3$). Both of them are numerical results using a quantum computer simulator without circuit noise. (c),(d) The corresponding operator size for (a) and (b). The red lines are ED results and the dashed lines are the result of a quantum computer simulator by Bell measurements without circuit noise.

FIG. 3. (a) The Trotter errors with time for both the integrable system ($h_z = 0$) and quantum chaotic one ($h_z = 0.3$) with the Trotter step $r = 100$. (b) The Trotter errors with different Trotter steps for a total time $t = 2$.

in Fig. 2. For $h_z = 0$, the operator size shows an oscillation with time. For $h_z \neq 0$ (we chose $h_z = 0.3$), the operator size increases for a period and reaches saturation afterward, which is evidence of operator scrambling. In addition, the operator size distributions and their evolution with time are presented in Figs. 2(a) and 2(b), respectively. Note that the simulation results fit well with the exact diagonalization (ED) for the operator size growth, which verifies the quantum algorithm.

We now consider the Trotter errors. To implement the Hamiltonian evolution in $\hat{O}(t)$ on a digital quantum computer, a decomposition into sequences of one-qubit and two-qubit gates is necessary, and the Trotter error ε due to the decomposition is related to the evolution time t and the number of time slices (or Trotter steps) $r = t/dt$ used in the decomposition. For a generic quantum system, the relation is $\varepsilon = O(t^2/r)$. The Trotter error can be smaller for a specific Hamiltonian. For instance, for a Hamiltonian H with a partition into $H = H_1 + H_2$ that all terms in H_1 (or H_2) mutually commute, the Trotter error becomes $\varepsilon = O(\frac{nt}{r} + \frac{nt^3}{r^2})$ [42]. This is just the case for MFIM or TFIM, where the Hamiltonian can be written as $H_I = H_z + H_x$, with H_z and H_x consisting of Z and X operators, respectively. The Trotter error $\varepsilon_{\mathrm{op}}$ for the operator $\sigma_\alpha^k(t) = U^\dagger(t)\sigma_\alpha^k(0)U(t)$ is $\varepsilon_{\mathrm{op}} \sim \varepsilon$, which turns to be

$$\varepsilon_{\mathrm{op}} \sim O\left(\frac{t}{r} + \frac{t^3}{r^2}\right). \tag{17}$$

Notably, the Trotter error is demonstrated by $O(\frac{t}{r})$ for small t. To verify the behavior of the Trotter error, we consider a maximum evolution time $T = 10$. The number of Trotter steps is fixed, $r = 100$. By simulation, the Trotter errors with time are shown in Fig. 3(a) (the fitting function is marked), which are in agreement with the theoretical analysis in Eq. (17). In addition, the behaviors of the Trotter errors with the number of time slices are shown in Fig. 3(b) for $t = 2$ [at $t = 2$, the
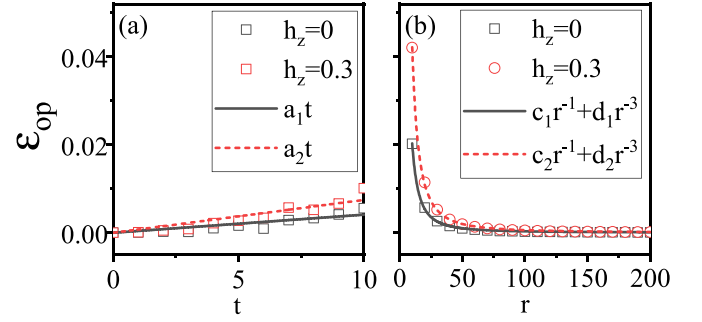
operator size ceases to increase, as seen in Figs. 2(c) and 2(d)]. Again, the simulation results are in agreement with the theoretical analysis in Eq. (17) [the fitting function is marked in Fig. 3(b)].

To implement the quantum algorithm on near-term quantum processors, the effects of quantum noise cannot be ignored [43]. For this, we continue to include quantum noise in the numerical simulation. As for a demonstration, we chose a noise model with depolarizing noise. The depolarizing noise model can be effective for large-size quantum circuits. During the simulation, the number of Trotter steps is set as $r = t/0.1$ and the noise of depolarization is added to each qubit after a quantum gate with a noise rate p. For a single qubit, the depolarization will evolve a density matrix ρ to ρ' as

$$\rho' = \frac{p}{3}(X\rho X + Y\rho Y + Z\rho Z) + (1-p)\rho. \tag{18}$$

To see the effects of depolarizing noise on the operator size, it is useful to consider a quantum operation of depolarizing on one qubit of the Bell state $|B^0\rangle$. The final state will be a mixed state of all four Bell states, $\frac{p}{3}(B^1 + B^2 + B^3) + (1 - p)B^0$, where we have short-noted $B^k = |B^k\rangle\langle B^k|$. Similarly, for Bell state $|B^1\rangle$, the mixed state after depolarization becomes $\frac{p}{3}(B^0 + B^2 + B^3) + (1 - p)B^1$. Corresponding to Pauli operators, it can be seen that the probability of turning an identity I into Pauli operators $\{X, Y, Z\}$ is p, while the probability of turning a Pauli operator into I is $\frac{p}{3}$. In this regard, depolarizing noise tends to increase the local operator density and thus the operator size.

As shown in Figs. 4(a) and 4(b), the distinction of the behavior of operator size growth can still be identified between oscillation and saturation behaviors when the depolarizing noise rate is a small one, e.g., $p \leqslant 10^{-4}$. However, for the larger noise rate $p \sim 10^{-3}$, which is comparable to real quantum hardware, the operator size reaches saturation for both integrable and chaotic systems. As analyzed before, the depolarizing noise can also increase the operator size, and it is hard to tell the oscillation and saturation behaviors of the operator growth apart, even when the noise rate is large compared to NISQ quantum devices. Thus, to simulate quantum chaotic systems by studying the operator size growth on real quantum processors, it is demanding to correct the errors or reduce the effects of noise.
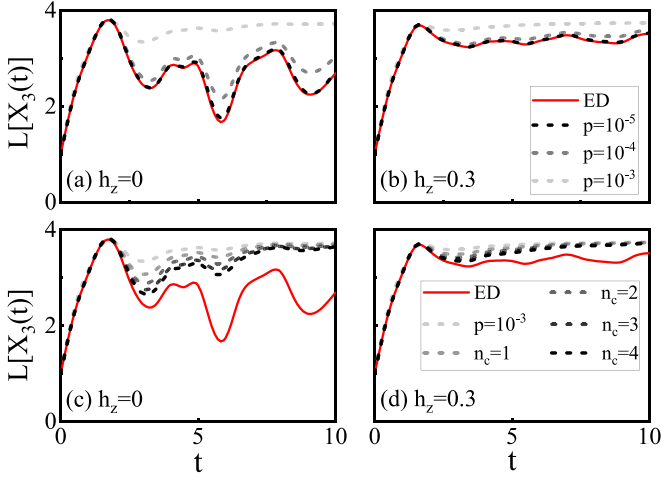
FIG. 4. Noise effects and error mitigation for the operator size growth. (a),(b) The operator size of $X_3(t)$ for the integrable system and chaotic one with different depolarizing noise rates. (c),(d) Results of error mitigation for (a) and (b), respectively, by extrapolation to the zero-noise limit with different n_c for a noise rate $p = 10^{-3}$.

Quantum error correction can provide an ultimate solution for handling quantum noise [44–47] and there has been rapid progress in experiments recently. Due to limited quantum resources, a practical way is to reduce noise effects by error-mitigation techniques. We adopt an error-mitigation technique by extrapolating to the zero-noise limit with Richardson's deferred method [33] (see the Appendix), which is suitable for short-depth quantum circuits. This can be achieved by performing quantum computing at several different noise rates with a scaling $p_j = c_j p$, where p is the lowest noise rate feasible on the quantum hardware and c_j is the scaling factor, and then make a linear combination of results with a weighting γ_j for the noise rate p_j and make extrapolation to the zero-noise limit. The parameters c_j and γ_j should satisfy two relations,

$$\sum_{j=0}^{n_c} \gamma_j = 1,$$

$$\sum_{j=0}^{n_c} \left(\gamma_j c_j^k \right) = 0 \quad \text{for} \quad k = 1, 2, \ldots, n_c, \quad (19)$$

and the error can be reduced to $O(p^{n_c+1})$. We chose parameters c_j and γ_j for different n_c: $c_0 = 1, c_1 = 2, \gamma_0 = 2, \gamma_1 = -1$ for $n_c = 1$; $c_0 = 1, c_1 = 2, c_2 = 3, \gamma_0 = 3, \gamma_1 = -3, \gamma_2 = 1$ for $n_c = 2$; $c_0 = 1, c_1 = 2, c_2 = 3, c_3 = 4, \gamma_0 = 4, \gamma_1 = -6, \gamma_2 = 4, \gamma_3 = -1$ for $n_c = 3$; and $c_0 = 1, c_1 = 2, c_2 = 3, c_3 = 4, c_4 = 5, \gamma_0 = 5, \gamma_1 = -10, \gamma_2 = 10, \gamma_3 = -5, \gamma_4 = 1$ for $n_c = 4$. As seen in Figs. 4(c) and 4(d), simulation results after error mitigation get better as n_c increase when the evolution time is not too long, which is expected as the corresponding quantum circuit depth is short.

Notably, the oscillation behavior of operator size growth, which is lost at a noise rate $p = 10^{-3}$, restores after error mitigation with $n_c = 3, 4$. This suggests that error mitigation can be an important ingredient for simulating and studying operator scrambling on near-term quantum devices.

IV. CONCLUSION

In summary, we have proposed a quantum algorithm to evaluate the operator size for quantum systems, which can be useful to study operator scrambling on near-term quantum devices by investigating the operator size growth. By preparing a product of Bell states as the initial state, the information of the operator in terms of a Pauli basis will be revealed in the Bell basis, and the operator size and its distribution can be extracted with Bell measurements. For implementing the quantum algorithm, we have considered both the Trotter errors due to the decomposition of the Hamiltonian evolution and the effects of quantum noise. We have demonstrated with numerical simulations that error mitigation is necessary for showing the oscillation and saturation behaviors of the operator growth separately on noisy quantum devices. Our work has suggested a feasible scheme for studying operator scrambling on near-term quantum computers by measuring the operator size growth.

APPENDIX: QUANTUM ERROR MITIGATION

Following Ref. [33], we give a short description of error mitigation by zero-noise extrapolation with Richardson's deferred method. For a noise-free system, the density matrix $\rho_0(T)$ satisfies the equation of motion

$$-i\hbar \frac{\partial \rho_0(T)}{\partial t} = [\hat{H}, \rho_0(T)], \quad (A1)$$

which determines $\rho_0(T) = \rho_0(0) + \frac{i}{\hbar} \int_0^T [\hat{H}, \rho_0(t)] dt$. The expectation value of operator $\hat{A}$ can be read as $E_0(T) = \text{tr}[\hat{A}\rho_0(T)]$.

When the noisy errors are introduced to the system with a noise rate p, the expectation value of operator $\hat{A}$ can be rewritten as

$$E_p(T) = \text{tr}[\hat{A}\rho_0(T)] + \sum_{k=1}^{n} a_k p^k + R_{n+1}(p, T), \quad (A2)$$

where a_k is the coefficients of the p^k and $R_{n+1}(p, T)$ is the higher-order p error. By considering the noises scaling $p_j = c_j p$, one can get

$$E_{p_j}(T) = \text{tr}[\hat{A}\rho_0(T)] + \sum_{k=1}^{n} a_k c_j^k p^k + R_{n+1}(c_j p, T). \quad (A3)$$

Thus, one can obtain the mitigation result by calculation,

$$
\begin{aligned}
E_p^{n_c}(T) &= \sum_{j=0}^{n_c} [\gamma_j E_{p_j}(T)] \\
&= \sum_{j=0}^{n_c} \gamma_j \left[E_0(T) + \sum_{k=1}^{n_c} a_k c_j^k p^k + R_{n_c+1}(c_j p, T) \right] \\
&= \sum_{j=0}^{n_c} \gamma_j E_0(T) + \sum_{j=0}^{n_c} \gamma_j \sum_{k=1}^{n_c} a_k c_j^k p^k \\
&\quad + \sum_{j=0}^{n_c} \gamma_j R_{n_c+1}(c_j p, T) \\
&= \left(\sum_{j=0}^{n_c} \gamma_j \right) E_0(T) + \sum_{k=1}^{n_c} \left(\sum_{j=0}^{n_c} \gamma_j c_j^k \right) a_k p^k \\
&\quad + \sum_{j=0}^{n_c} \gamma_j R_{n+1}(c_j p, T).
\end{aligned}
\tag{A4}
$$

The above equation (A4) shows that the noisy error can be reduced to $\sum_{j=0}^{n_c} \gamma_j R_{n_c+1}(c_j p, T)$, by selecting a set of suitable c_j and γ_j. Both c_j and γ_j should satisfy

$$
\sum_{j=0}^{n_c} \gamma_j = 1,
$$

$$
\sum_{j=0}^{n_c} (\gamma_j c_j^k) = 0 \quad \text{for} \quad k = 1, 2, \ldots, n_c.
\tag{A5}
$$

Then, the mitigation result can be rewritten as

$$
E_p^{n_c}(T) = E_0(T) + \sum_{j=0}^{n_c} \gamma_j R_{n_c+1}(c_j p, T).
\tag{A6}
$$

The optimization result shows that the error reduces to $\sum_{j=0}^{n_c} \gamma_j R_{n_c+1}(c_j p, T)$.

---

[1] M. Srednicki, Phys. Rev. E **50**, 888 (1994).

[2] A. Bohrdt, C. B. Mendl, M. Endres, and M. Knap, New J. Phys. **19**, 063001 (2017).

[3] A. Chan, A. De Luca, and J. T. Chalker, Phys. Rev. X **8**, 041019 (2018).

[4] B. Swingle, G. Bentsen, M. Schleier-Smith, and P. Hayden, Phys. Rev. A **94**, 040302(R) (2016).

[5] A. A. Patel, D. Chowdhury, S. Sachdev, and B. Swingle, Phys. Rev. X **7**, 031047 (2017).

[6] S. Pappalardi, A. Russomanno, B. Žunkovič, F. Iemini, A. Silva, and R. Fazio, Phys. Rev. B **98**, 134303 (2018).

[7] T. Ali, A. Bhattacharyya, S. S. Haque, E. H. Kim, N. Moynihan, and J. Murugan, Phys. Rev. D **101**, 026021 (2020).

[8] T. Xu, T. Scaffidi, and X. Cao, Phys. Rev. Lett. **124**, 140602 (2020).

[9] M. K. Joshi, A. Elben, B. Vermersch, T. Brydges, C. Maier, P. Zoller, R. Blatt, and C. F. Roos, Phys. Rev. Lett. **124**, 240505 (2020).

[10] X. Mi, P. Roushan, C. Quintana, S. Mandrà, J. Marshall, C. Neill, F. Arute, K. Arya, J. Atalaya, R. Babbush, J. C. Bardin, R. Barends, J. Basso, A. Bengtsson, S. Boixo, A. Bourassa, M. Broughton, B. B. Buckley, D. A. Buell, B. Burkett, N. Bushnell, Z. Chen, B. Chiaro, R. Collins, W. Courtney, S. Demura, A. R. Derk, A. Dunsworth, D. Eppens, C. Erickson, E. Farhi, A. G. Fowler, B. Foxen, C. Gidney, M. Giustina, J. A. Gross, M. P. Harrigan, S. D. Harrington, J. Hilton, A. Ho, S. Hong, T. Huang, W. J. Huggins, L. B. Ioffe, S. V. Isakov, E. Jeffrey, Z. Jiang, C. Jones, D. Kafri, J. Kelly, S. Kim, A. Kitaev, P. V. Klimov, A. N. Korotkov, F. Kostritsa, D. Landhuis, P. Laptev, E. Lucero, O. Martin, J. R. McClean, T. McCourt, M. McEwen, A. Megrant, K. C. Miao, M. Mohseni, S. Montazeri, W. Mruczkiewicz, J. Mutus, O. Naaman, M. Neeley, M. Newman, M. Y. Niu, T. E. O'Brien, A. Opremcak, E. Ostby, B. Pato, A. Petukhov, N. Redd, N. C. Rubin, D. Sank, K. J. Satzinger, V. Shvarts,

D. Strain, M. Szalay, M. D. Trevithick, B. Villalonga, T. White, Z. J. Yao, P. Yeh, A. Zalcman, H. Neven, I. Aleiner, K. Kechedzhi, V. Smelyanskiy, and Y. Chen, Science **374**, 1479 (2021).

[11] S. H. Shenker and D. Stanford, J. High Energy Phys. 03 (2014) 067.

[12] S. H. Shenker and D. Stanford, J. High Energy Phys. 12 (2014) 046.

[13] J. Li, R. Fan, H. Wang, B. Ye, B. Zeng, H. Zhai, X. Peng, and J. Du, Phys. Rev. X **7**, 031011 (2017).

[14] C.-J. Lin and O. I. Motrunich, Phys. Rev. B **97**, 144304 (2018).

[15] C. W. von Keyserlingk, T. Rakovszky, F. Pollmann, and S. L. Sondhi, Phys. Rev. X **8**, 021013 (2018).

[16] W.-L. Zhao, Y. Hu, Z. Li, and Q. Wang, Phys. Rev. B **103**, 184311 (2021).

[17] T. Rakovszky, F. Pollmann, and C. W. von Keyserlingk, Phys. Rev. X **8**, 031058 (2018).

[18] V. Balachandran, G. Benenti, G. Casati, and D. Poletti, Phys. Rev. B **104**, 104306 (2021).

[19] B. Vermersch, A. Elben, L. M. Sieberer, N. Y. Yao, and P. Zoller, Phys. Rev. X **9**, 021061 (2019).

[20] J. Harris, B. Yan, and N. A. Sinitsyn, Phys. Rev. Lett. **129**, 050602 (2022).

[21] P. Hosur and X.-L. Qi, Phys. Rev. E **93**, 042138 (2016).

[22] D. A. Roberts, D. Stanford, and A. Streicher, J. High Energy Phys. 06 (2018) 122.

[23] A. Nahum, S. Vijay, and J. Haah, Phys. Rev. X **8**, 021014 (2018).

[24] V. Khemani, A. Vishwanath, and D. A. Huse, Phys. Rev. X **8**, 031057 (2018).

[25] S. Gopalakrishnan, D. A. Huse, V. Khemani, and R. Vasseur, Phys. Rev. B **98**, 220303(R) (2018).

[26] X.-L. Qi and A. Streicher, J. High Energy Phys. 08 (2019) 012.

[27] X.-L. Qi, E. J. Davis, A. Periwal, and M. Schleier-Smith, arXiv:1906.00524.

[28] S. Moudgalya, T. Devakul, C. W. von Keyserlingk, and S. L. Sondhi, Phys. Rev. B **99**, 094312 (2019).

[29] D. E. Parker, X. Cao, A. Avdoshkin, T. Scaffidi, and E. Altman, Phys. Rev. X **9**, 041017 (2019).

[30] S. K. Zhao, Z.-Y. Ge, Z. Xiang, G. Xue, H. S. Yan, Z. T. Wang, Z. Wang, H. K. Xu, F. Su, Z. H. Yang, H. Zhang, Y.-R. Zhang, X. Guo, K. Xu, Y. Tian, H. F. Yu, D. N. Zheng, H. Fan,and S. P. Zhao, Phys. Rev. Lett. **129**, 160602 (2022).

[31] T. Schuster and N. Y. Yao, arXiv:2208.12272.

[32] E. McCulloch and C. W. von Keyserlingk, J. Phys. A: Math. Theor. **55**, 274007 (2022).

[33] K. Temme, S. Bravyi, and J. M. Gambetta, Phys. Rev. Lett. **119**, 180509 (2017).

[34] S. Endo, S. C. Benjamin, and Y. Li, Phys. Rev. X **8**, 031027 (2018).

[35] M. S. Jattana, F. Jin, H. D. Raedt, and K. Michielsen, Quantum Inf. Proc. **19**, 414 (2020).

[36] A. Strikis, D. Qin, Y. Chen, S. C. Benjamin, and Y. Li, PRX Quantum **2**, 040330 (2021).

[37] E. R. Bennewitz, F. Hopfmueller, B. Kulchytskyy *et al.*, Nat. Mach. Intell. **4**, 618 (2017).

[38] Y. Suzuki, S. Endo, K. Fujii, and Y. Tokunaga, PRX Quantum **3**, 010345 (2022).

[39] S. Chen, S. Zhou, A. Seif, and L. Jiang, Phys. Rev. A **105**, 032435 (2022).

[40] H.-Y. Huang, M. Broughton, J. Cotler, S. Chen, J. Li, M. Mohseni, H. Neven, R. Babbush, R. Kueng, J. Preskill, and J. R. McClean, Science **376**, 1182 (2022).

[41] T. Haug and M. S. Kim, PRX Quantum **4**, 010301 (2023).

[42] M. C. Tran, S.-K. Chu, Y. Su, A. M. Childs, and A. V. Gorshkov, Phys. Rev. Lett. **124**, 220502 (2020).

[43] J. Preskill, Quantum **2**, 79 (2018).

[44] P. W. Shor, Phys. Rev. A **52**, R2493 (1995).

[45] A. M. Steane, Phys. Rev. Lett. **77**, 793 (1996).

[46] D. Gottesman, arXiv:0904.2557.

[47] D. F. V. James, Phys. Today **54**(11), 60 (2001).